Paper M

DIFFRACTION TOMOGRAPHY OF STRONGLY SCATTERING MEDIUM PART I: USING PHASE EXTRAPOLATION

Guan Y. Wang

ABSTRACT

The existing diffraction tomographic techniques are mainly based on the Born approximation. Such methods are simple to implement but do not work well in a strongly scattering medium. We re-exam the widely used inverse scattering model and develop a formulation to include multiple scattering by estimating the scattered field inside the medium with the Fourier phase extrapolation technique. The method works well in the situation where the variation of the propagation speed due to inhomogeneity is small. The yield algorithm is the same as conventional diffraction tomography with the Born approximation. However, the individual diffraction projection of the scattering spectrum is obtained by solving the Toeplitz recursive equation in the transform domain.

INTRODUCTION

Diffraction tomography is used to reconstruct, from the observed scattered field, the spatial distribution of appropriate parameters in a medium. In its common form, diffraction tomography is formulated as an approximate inversion of the Helmholtz equation with a spatially varying coefficient. The inversion is accomplished in practice by first transforming the Helmholtz equation into an inhomogeneous one with constant coefficients. Two transformations leading to two different approximate inversions have been most commonly used, i.e., the Born and Rytov transformations (Devaney, 1984; Harris, 1987). See Appendix A for a summary about the Born approximation. These techniques substantially simplify the inversion problem and all for computational advantages of fast Fourier transform processing. The appealing feature of these methods is the fact that the inversion algorithms are non-iterative and computationally efficient. However, computational efficiency and algorithmic simplicity are accompanied by limitations on the ranges of validity for these methods.

The objective of this study is to reformulate the basic diffraction tomography algorithms to include the effects of multiple scattering. Therefore, the diffraction tomography methods will be able to work in strongly inhomogeneous medium. To take account the multiple scattering, the total field in the integral kennel is estimated by phase extrapolation or other techniques. In this paper, we present a formulation in which the total field is estimated with the Fourier phase extrapolation and the individual diffraction projection of the scattering spectrum from the receiver gather. This is obtained by solving the Toeplitz recursive equation. Once the spectrum of the object is obtained, the object function is reconstructed by the inverse Fourier transform.

TIME HARMONIC SOLUTIONS

Fourier integral techniques provide the most powerful method of analysis of wave propagation problems. By use of superposition it is possible to express a wave pulse as a superposition in frequency space of harmonic motions.

$$(\nabla^2 + k^2)\phi(r) = v(r)\psi(r), \tag{1}$$

where ψ and ϕ are the total and scattered fields respectively. $k = \omega / v_0$ and $v = k^2 o(r)$. Notice that ω is angular frequency, v_0 the background velocity and o the strength of scatterer. The solution to equation (1) can be expressed as Lippmann-Schwinger integral equation,

$$\psi(r) = \varphi(r) + \int dr' \, G(r - r')v(r')\psi(r'). \tag{2}$$

The asymptotic form of the wave function is

$$\psi(r) \rightarrow \varphi(r) + f(k,k')\frac{\exp(ikr)}{r}$$

$$f(k,k') = -\int dr' \, e^{-ik'\cdot r} v(r')\psi(r')$$

the coefficient f(k,k') of the outgoing wave is usually called the scattering amplitude. Notice that the scattering amplitude f(k,k') depends on the energy of the relative motion, the angle between the vector k and k', and the scattering potential. To calculate the scattering amplitude, it is necessary to know the solution of equation (2).

SPECTRUM REPRESENTATION

Equation (2) can be rewritten as two parts

$$\varphi(g,s) = -\int G(g,r)v(r)G(r,s)d^2r - \int G(g,r)v(r)\varphi(r,s)d^2r. \tag{3}$$

The second term on the right hand of the equation (3) is the multiple scattering term which is responsible for the nonlinear effects of the interaction between scattered and multiple scattering waves, as indicated in figure 1.

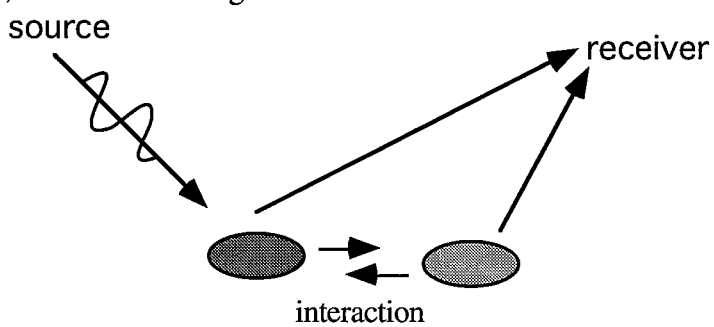

Figure 1. Illustration of scattering and multiple scattering.

For two dimensional problem, the Green's function in equation (3) is the first kind and zero order Hankel function, i.e.

$$G(r,s)=\frac{i}{4}H_0^{(1)}(k|r-s|),\ \text{and}\ \ G(g,r)=\frac{i}{4}H_0^{(1)}(k|g-r|).$$

The spectra of the 2-D Green's function along the source line and receiver line can be given by

$$G(r,k_s)=\frac{i}{2\gamma_s}\exp(i\gamma_s x_s)\exp(ik\hat{s}\cdot r),$$

and

$$G(k_g,r)=\frac{i}{2\gamma_g}\exp(-i\gamma_g x_g)\exp(-ik\hat{g}\cdot r),$$

which are in the form of a plane wave. After plane wave decomposition, the spectrum representation of equation (3) take the form of

$$\begin{aligned}\Phi(x_g,k_g|x_s,k_s)=&\frac{\exp(-i\gamma_g x_g+i\gamma_s x_s)}{4\gamma_g\gamma_s}\int v(x,z)\exp\{-i[(\gamma_g-\gamma_s)x+(k_g+k_s)z]\}dxdz\\&-\frac{i\exp(-i\gamma_g x_g)}{2\gamma_g}\int v(x,z)\varphi(x,z|x_g,k_s)\exp[-i(\gamma_g x-k_g z)]dxdz\end{aligned}\qquad(4)$$

The scattered field at the observation locations is expressed as $\phi(x_g,z_g|x_s,z_s)$, and its spectrum is denoted as $\Phi(x_g,k_g|x_s,k_s)$. For many situations where the inhomogeneity, i.e., the scatterers are local concentrations, we can extrapolate the wave field approximately with a constant background velocity, as in the case of Fourier phase migration (Stolt, 1978), to obtain the scattering field at an arbitrary location, i.e.

$$\Phi(x,z|x_s,k_s)=\frac{1}{2\pi}\int\Phi(x_g,k_g|x_s,k_s)e^{i(\gamma_g x+k_g z)}dk_g,\qquad(5)$$

where $\gamma_g=\sqrt{k_0^2-k_g^2}$ is the horizontal wave number. By noticing that the integrals on the right side of equation (5) are Fourier transforms, and substituting equation (5) into (4), we have

$$\begin{aligned}&\Phi(x_g,k_g|x_s,k_s)=A(\gamma_g,\gamma_s)V(\gamma_g-\gamma_s,k_g+k_s)-\\&\frac{B(\gamma_g)}{2\pi}\int dk''\varphi(x_g,k''|x_s,k_s)e^{-i\gamma'' x_g}\int v(x,z)e^{-i[(\gamma_g-\gamma'')x+(k_g-k'')z]}dxdz\end{aligned}$$

or

$$\Phi(x_g,k_g|x_s,k_s) = A(\gamma_g,\gamma_s)V(\gamma_g-\gamma_s,k_g+k_s) + \\ -\frac{B(\gamma_g)}{2\pi}\int dk''\,\varphi(x_g,k''|x_s,k_s)e^{-i\gamma''x_g}V(\gamma_g-\gamma'',k_g-k''), \tag{6}$$

where

$$A(\gamma_g,\gamma_s) = \frac{\exp(-i\gamma_g x_g + i\gamma_s x_s)}{4\gamma_g\gamma_s},$$

$$B(\gamma_g) = \frac{i\exp(-i\gamma_g x_g)}{2\gamma_g}.$$

By defining $D_{k_s}(k_g) = \dfrac{\Phi(x_g,x_g|x_s,k_s)}{A(\gamma_s,\gamma_g)}$, the notations in equation (6) can be simplified as

$$D_{k_s}(k_g) = V(\gamma_g-\gamma_s,k_g+k_s) \\ -\frac{i\gamma_s\exp(-i\gamma_s x_s)}{\pi}\int dk''\,\varphi(x_g,k''|x_s,k_s)e^{-i\gamma''x_g}V(\gamma_g-\gamma'',k_g-k''), \tag{7}$$

or further simplified as

$$D_{k_s}(k_g) = V_{k_s}(k_g) - \frac{i\exp(-i\gamma_s x_s)}{\pi}\int dk''\,\varphi_{k_s}(k'')V_{k_s}(k_g-k''), \tag{8}$$

where

$$V_{k_s}(k_g) = V(\gamma_g-\gamma_s,k_g+k_s),$$

$$V_{k_s}(k_g-k'') = V(\gamma_g-\gamma'',k_g-k''),$$

and

$$\Phi_{k_s}(k'') = \Phi(x_g,k''|x_s,k_s)e^{-i\gamma''x_g}.$$

Equation (8) is a convolution integral with the kennel of the scattered field spectrum. Notice that when the strength of the scatterer is weak, only the first term on the right side of the equation is used which is the Born approximation. However, for arbitrary scatterers, multiple scattering can be strong. The convolution integral in equation (8) can not be ignored and the linear relation under the Born approximation is broken. We will show in equation (8), V_{k_s} is a single diffracted projection for a fixed wavenumber k_s,. This is independent to other projections with different wavenumber k_s. Therefore, we can solve for them independently.

NONLINEAR DIFFRACTION PROJECTIONS

Equation (8) can be rewritten as

$$D_{k_s}(k_g) = V_{k_s}(k_g) - \frac{i\exp(-i\gamma_s x_s)}{\pi}\int dk''\,\varphi_{k_s}(k_g - k'')V_{k_s}(k''). \qquad (9)$$

For a fixed k_S, the above Toeplitz linear system can be solved for one trace of the scattering spectrum V as indicated in Figure 2a.

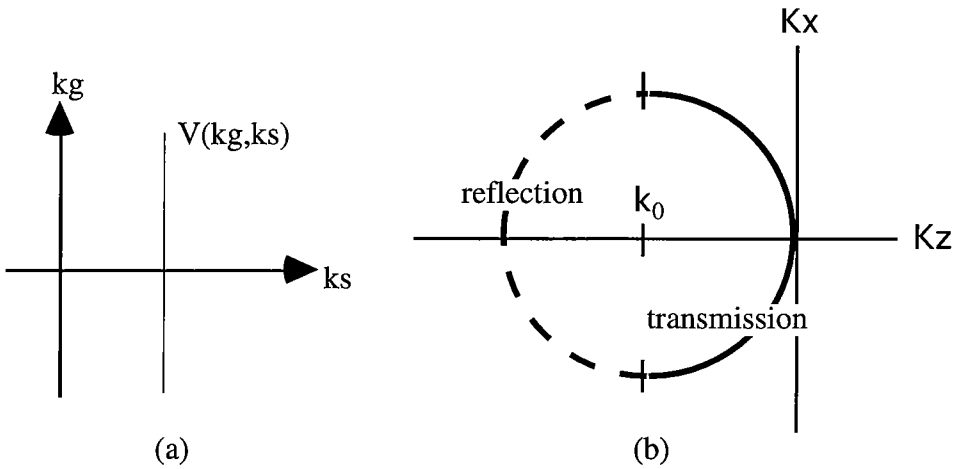

Figure 2. Fourier transform of the nonlinear diffraction projection; (a) the projection in k_g–k_S domain, and (b) the projection in K_X-K_Z domain.

With a Jacobean transformation, the above linear trace of scatter spectrum in k_g–k_S becomes a curve in K_X-K_Z domain, see Figure 2 (b). We represent the discrete form of equation (13) as

$$D_{k_s}(m) = \sum_n [\delta(m-n) - \frac{i\exp(-i\gamma_s x_s)}{\pi}\varphi_{k_s}(m-n)\Delta k'']V_{k_s}(n). \qquad (14)$$

The system in equation (14) is a Toeplitz type and the matrix elements consist with Fourier coefficients of the observed scattered field, i.e.,

$$\begin{bmatrix} 1 - i\Phi_{k_s}(0)/\pi & \Phi_{k_s}(-1) & \cdots & \Phi_{k_s}(-n) \\ \Phi_{k_s}(1) & 1 - i\Phi_{k_s}(0)/\pi & & \Phi_{k_s}(1-n) \\ \vdots & & & \vdots \\ \Phi_{k_s}(n) & \Phi_{k_s}(n-1) & \cdots & 1 - i\Phi_{k_s}(0)/\pi \end{bmatrix}.$$

NUMERICAL EXPERIMENTS

Figure 3a shows the velocity field used for the two-dimensional experiment: An anomalous circular region 20 m in diameter with a velocity of 5000 m/sec is located at the center of the medium. The background velocity is 3000 m/sec. The synthetic data are calculated with the analytical expression in Appendix B. The frequency used is 1000 Hz. The calculated scattering field is shown in figure 3b and we can see that the scattering field is stronger in the forward direction. The spectrum difference between the Born approximation and the nonlinear diffraction projection is shown in figure 4.

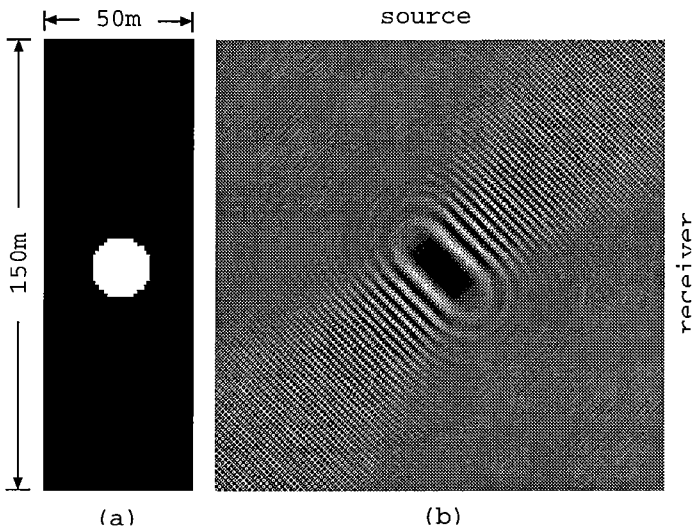

Figure 3. Synthetic data modeling using the analytical formula: a) a disk model; b) scattering data (real part). Frequency=1000Hz.

The largest difference (around ten percent) occurred at the highest frequency which is expected, Since the multiple scattering has the higher frequencies. It is shown in figure 5 that the shape reconstruction is quite good using both the Born approximation and nonlinear projection methods. Note that the disk is elongated in the x direction, both in figure 5b and 5c, as is expected since the resolution is poorer in that direction. Compared to the result using the Born approximation, the velocity reconstruction with the nonlinear projection algorithm has significantly improved (figure 5c).

In the second example, the model has a background velocity of 3500 m/sec and two linear velocity abnormal features of 5000 m/sec representing fracture zones (Figure 6a). The moment method is used to generate forward data (Appendix C). A 50 m horizontal by 150 m vertical area is considered with a sampling interval of 0.5 m. The frequency is 1000Hz.

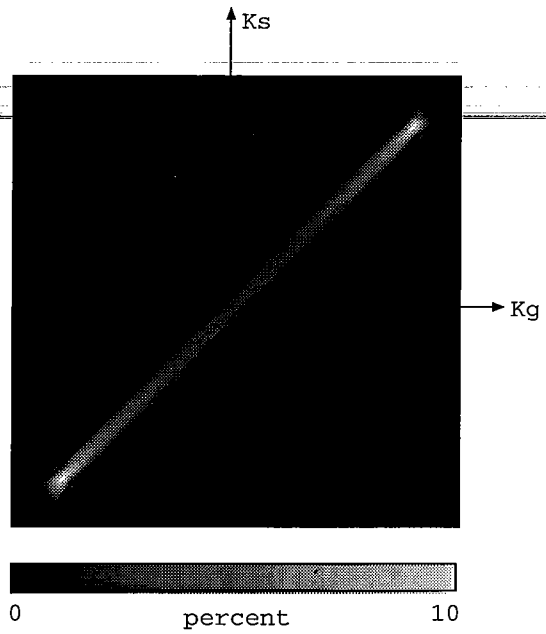

Figure 4. The spectrum difference between the linear and nonlinear projection. The largest difference occurred at high frequencies. The scattered field is from the synthetic data of the disk model.

The calculated scattering field (real part) is shown in figure 6b. The scattering spectra from the Born approximation and nonlinear diffraction projections are shown in figure 7. Once again we see the difference at high frequencies. The inversion results are shown in figure 8b and 8c. We can see that the diffractor lines are thicker comparing to input model and the

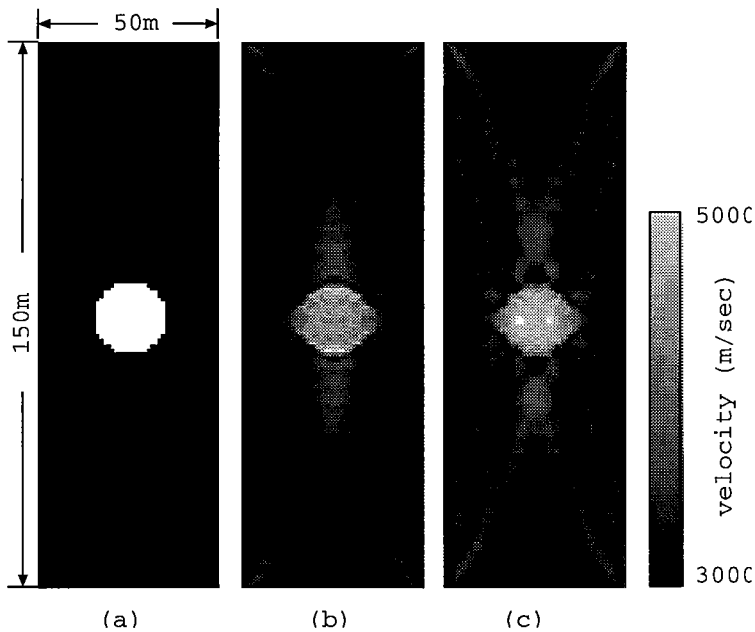

Figure 5. A comparison between the Born approximation and nonlinear projection diffraction tomography. a) A disk mode; b) the reconstruction with linear projection; c) the reconstruction with nonlinear projection.

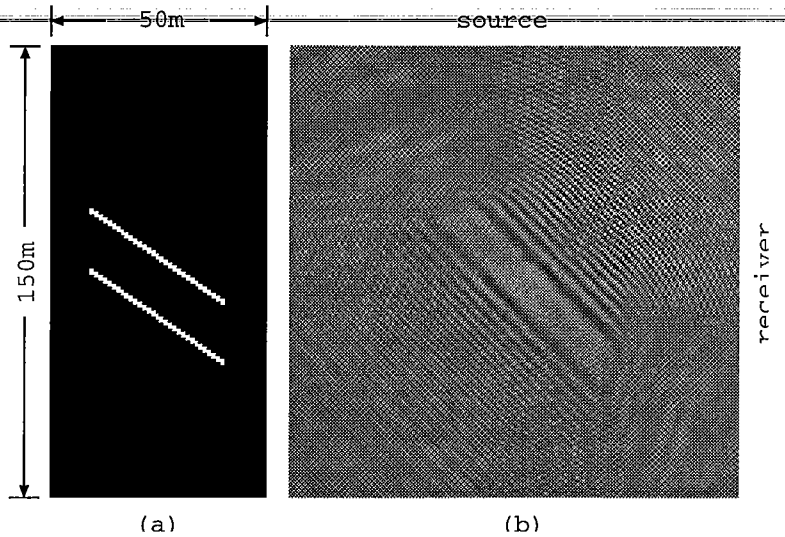

Figure 6. Synthetic data generated using the moment method: a) a fracture model; b) scattering data (real part). Frequency = 1000Hz.

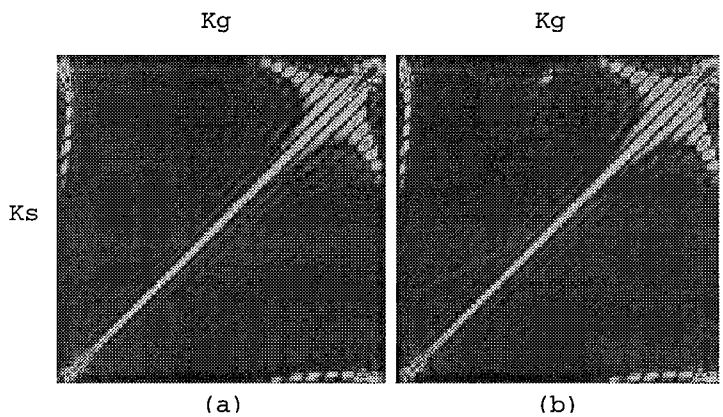

Figure 7. The spectrum of the scattered field with the linear and nonlinear diffraction projections. a) The spectrum with Born approximation; and b) the spectrum with nonlinear diffraction projection.

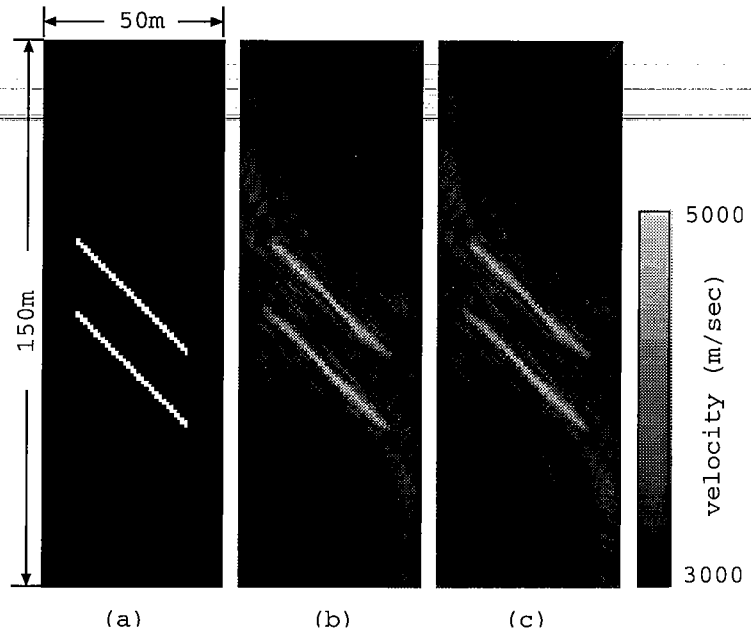

Figure 8. A comparison between the linear and nonlinear projection diffraction tomography. a) Fracture mode; b) the reconstruction with linear projection; and c) the reconstruction with nonlinear nonlinear projection.

diffractor lines are not as distinctly resolved in comparison with the original image. This is caused by the wavenumber domain coverage being constrained to low wavenumbers in the crosswell case. In this example, the reconstructed images with the Born approximation and nonlinear projection has little difference, since the multiple scattering is insignificant in the forward direction.

The last example is to test the quality of imaging for complex structure. The model consists three letters "STP" as the object to be reconstructed . The letters are consists of point scatters, see figure 9a. The sources and receivers are equally spaced at half wavelength intervals. Figure 9b shows the results from nonlinear projection diffraction tomography. The locations of the letters are correctly recovered. The distortion is possibly caused by inaccuracy of synthetic data modeling with the moment method at high frequencies (1500 Hz).

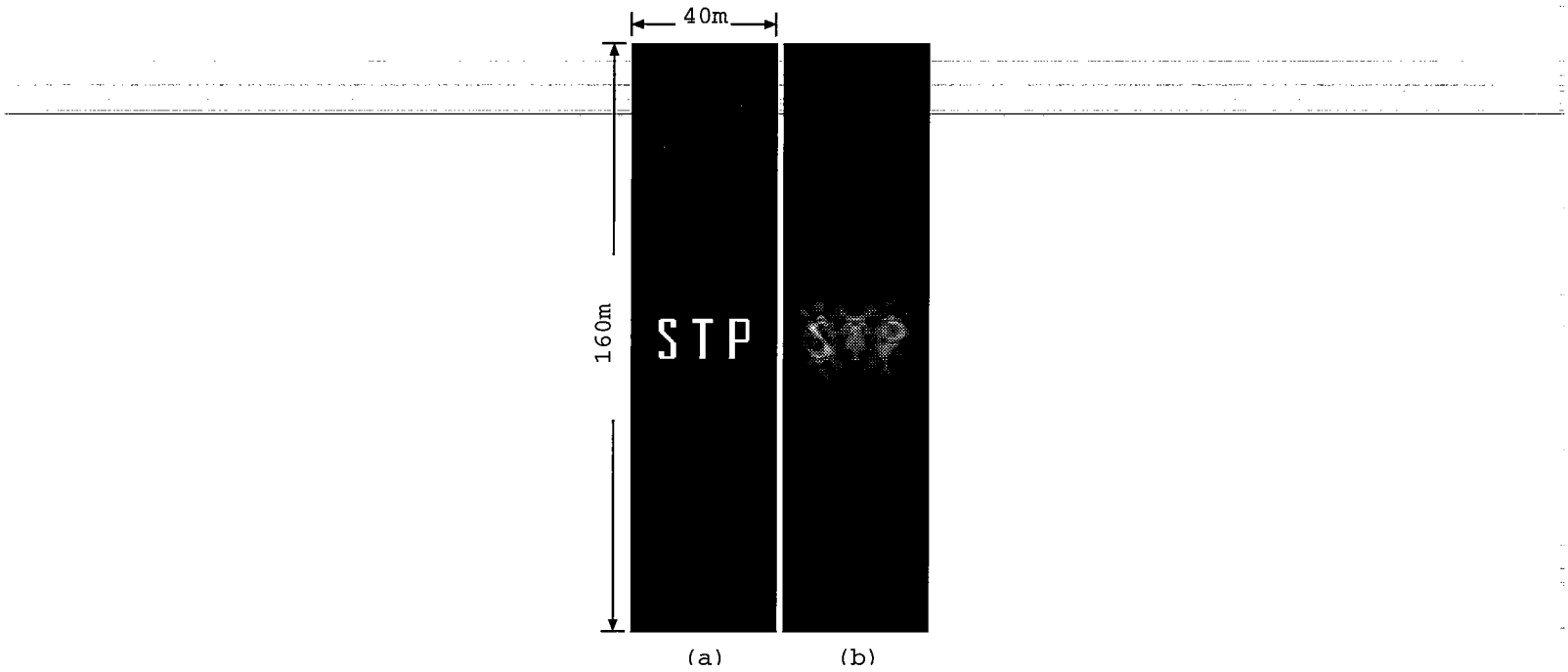

Figure 9. The reconstruction with nonlinear projection diffraction tomography. The synthetic data is calculated with the moment method at frequency = 1500 Hz.

CONCLUSIONS

It is possible that the computational efficiency and simplicity of the traditional diffraction tomography can be preserved while the nonlinear effects of multiple scattering are taken into account. Numerical results indicate the improvement to the Born approximation for the models have strong scatterers. However, when the scale of the scatterers significantly influence the propagation of the scattered field, the phase extrapolation breaks down. The method yields an algorithm of asymptotic order $N^3 \log N$, where N is the number of sources and receivers. Reconstruction is efficient on a IBM RS6000 workstation, requiring only approximately 2 minutes for a single frequency when N=150.

ACKNOWLEDGEMENTS

The author thanks Nick Smalley for editing this paper.

REFERENCES

A. J. Devaney, Geophysical diffraction tomography, IEEE Trans. Geosci. Remote Sensing GE-22, 3-13 (1984)

J. M. Harris, Diffraction tomography imaging with arrays of source and detectors, IEEE Trans. Geoscience Remote Sensing, vol. Ge-25, No. 4, 448-455, 1987

R. H. Stolt, Migration by Fourier transform, Geophysics, 43, 23-28.

R. S. Wu and M. N. Toksoz, Diffraction tomography and multi-source holography applied to seismic imaging, Geophysics 52, 11-25 (1987)

APPENDIX A

A DESCRIPTION OF THE BORN APPROXIMATION

The solution to Homholtz equation can be expressed as integral equation:

$$\psi(r) = \varphi(r) + \int dr' \, G(r - r')v(r')\psi(r'). \tag{A-1}$$

The asymptotic form of the wave function is

$$\psi(r) \rightarrow \varphi(r) + f(k,k')\frac{\exp(ikr)}{r} \tag{A-2}$$

$$f(k,k') = -\int dr' \, e^{-ik'\cdot r} v(r')\psi(r'), \tag{A-3}$$

Replacing the exact wave function $\psi(r')$ by the incident wave $\varphi(r)$ we find the scattering amplitude in the Born approximation:

$$f(k,k') = -\int dr' \, e^{-ik'\cdot r} v(r')\varphi(r'), \tag{A-4}$$

Choosing plane waves for $\varphi(r)$, we can represent the scattering amplitude in the form

$$f(k,k') = -\int dr' \, e^{-iq\cdot r} v(r'), \tag{A-5}$$

where q is the change in the particle momentum on the scattering

$$q = k - k'. \tag{A-6}$$

The absolute magnitude of the vector q is

$$q = 2k\sin\frac{\theta}{2}, \tag{A-7}$$

where θ is the scattering angle (the angle between the vector k' and k). We can see that the scattering amplitude in the Born approximation is determined by the Fourier component of the scattering field and depends only on the magnitude of the transferred momentum q.

The scattering potential function can be reconstructed by taking the inverse Fourier transform of equation (A-5). The conditions for Born approximation to be valid can be summarized as: For low frequencies

$$\overline{V} << 1/R^2, \quad kR << 1. \tag{A-8}$$

This condition implies that for perturbation theory to be applicable, the effective value of the potential must be small in comparison with the wave length localized in the region of the influence of the potential. For high frequencies

$$\overline{V} << \frac{1}{R^2} kR, \quad kR >> 1. \tag{A-9}$$

We note that the condition (A-9) is considerably weaker than the condition (A-8).

APPENDIX B

AN ANALYTICAL SOLUTION OF THE FIELD SCATTED FROM A DISK

We designate the source and receiver coordinates to be (r', θ') and (r, θ) (see figure B-1). The density and velocity inside and outside the disk are given by (ρ, v) and (ρ_0, v_0). Assuming the incident field is the Hankel function,

$$\varphi(|x' - x|) = \frac{i}{4} H_0^{(1)}(k_0 |x' - x|), \tag{B-1}$$

which can be expanded as, for r < r',

$$\varphi(|x' - x|) = \frac{i}{4} \sum_n e^{-in(\theta' - \theta)} H_n^{(1)}(k_0 r') J_n(k_0 r), \tag{B-2}$$

where $H_n^{(1)}$ is the Hankel function of the first kind and nth order.

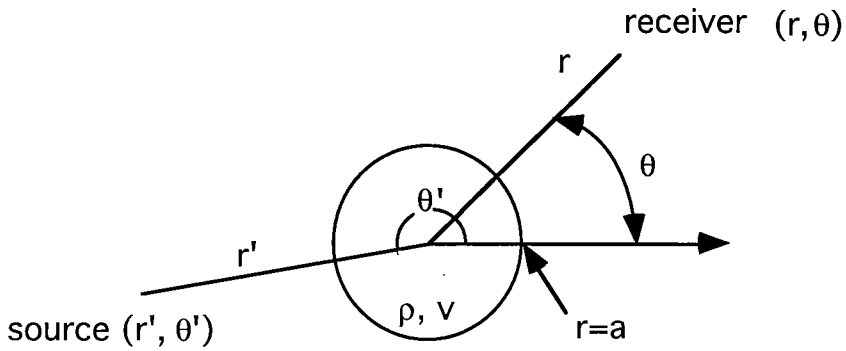

Figure A-1. The scattering geometry of a cylindrical disk.

The fields outside and inside the disk can be expressed as

$$\varphi_{out}(r) = \sum_n C_{out} e^{in\theta} H_n^{(1)}(k_0 r) \quad \text{and} \quad \varphi_{in}(r) = \sum_n C_{in} e^{in\theta} J_n(k_0 r) \tag{B-3}$$

The coefficients C_{in} and C_{out} are determined by using the boundary conditions for the problem, with require that $\rho\varphi$ and $\partial\varphi / \partial r$ be continuous at the surface of the disk. Applying these conditions we obtain the scattered field outside the disk:

$$\varphi_{out}(r) = \frac{i}{4} \sum_n e^{-in(\theta' - \theta)} H_n^{(1)}(k_0 r') H_n^{(1)}(k_0 r) A / B \tag{B-4}$$

where

$$A = \rho k_0 J_n(ka) \dot{J}_n(k_0 a) - \rho_0 k \dot{J}_n(ka) J_n(k_0 a),$$

$$B = \rho_0 k H_n^{(1)}(k_0 a) \dot{J}_n(ka) - \rho k_0 \dot{H}_n^{(1)}(k_0 a) J_n(ka).$$

The summation can be carry out over positive indices by using the index symmetry of the Bessel functions.

APPENDIX C

THE METHOD OF MOMENT

The moment method is often applied in calculation of the scattered field from the two dimensional inhomogeneity (Bath, 1982, Chew, 1990), such as described by the following equation:

$$u(r) = u^i - \int u(r')e(r')G(r,r')d^2r' \tag{C-1}$$

The method is straight forward and efficient when the size of the scatterer is small (i.e., the volume or area depending dimension of the problem is small.) The scattering region is region separated into N square cells (see figure C-1). Then, the scattering potential and wave field are represented as a summation of basis function over the N cells, i.e.,

$$e(r) = \sum_{j,k} e(r_{jk})b_{jk}(r)$$

$$u(r) = \sum_{j,k} a_{jk}b_{jk}(r) \tag{C-2}$$

where $b_{jk}(r)$ is the basis function, $e(r_{jk})$ and a_{jk} represent the coefficients describing the scattering potential and wave field over the basis function.

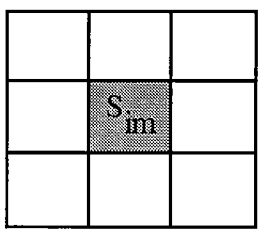

Figure C-1. Scattering potential is divided up into N square cells

We chose the same pulse basis function $b_{jk}(r)$ to discretize equation (C-1), i.e.,

$$b_{jk}(r) = \begin{cases} 1 & r \in s_{jk} \\ 0 & r \notin s_{jk} \end{cases} \tag{C-3}$$

Applying the point-matching procedure, the equation (5) can be written as a linear algiboal system, i.e.,

$$u_{jk} + \sum_{i,m} g(j,k,i,m)f(r_{im})u_{im} = G(r_{jk}), \tag{C-4}$$

where $g(j,k,i,m) = \int_{s_{im}} G(r_{jk})d^2r$.